Journal of Materials Chemistry C

ROYAL SOCIETY OF CHEMISTRY

PAPER

Cite this: J. Mater. Chem. C, 2021, 9, 6277

Anomalous Raman modes in tellurides†

Francisco Javier Manjón, *[a] Samuel Gallego-Parra, [a] Plácida Rodríguez-Hernández, [b] Alfonso Muñoz, [b] Cestmir Drasar, [c] Vicente Muñoz-Sanjosé [d] and Oliver Oeckler [e]

Received 2nd March 2021, Accepted 19th April 2021

DOI: 10.1039/d1tc00980j

rsc.li/materials-c

Two anomalous broad bands are usually found in the Raman spectrum of bulk and 2D Te-based chalcogenides, which include binary compounds, like ZnTe, CdTe, HgTe, GaTe, GeTe, SnTe, PbTe, $GeTe_2$, As_2Te_3, Sb_2Te_3, Bi_2Te_3, $NiTe_2$, $IrTe_2$, and $TiTe_2$, as well as ternary compounds, like GaGeTe, $SnSb_2Te_4$, $SnBi_2Te_4$, and $GeSb_2Te_5$. Many different explanations have been proposed in the literature for the origin of the anomalous broad bands in tellurides, usually located between 119 and 145 cm^{-1}. They have been attributed to the intrinsic Raman modes of the sample, to oxidation of the sample, to the folding of Brillouin-edge modes onto the zone center, to the existence of a double resonance, like that of graphene, or to the formation of Te precipitates. In this paper, we provide arguments to demonstrate that such bands correspond to clusters or precipitates of trigonal Te in the form of nanosize or microsize grains or layers that are segregated either inside or at the surface of the samples. Several mechanisms for Te segregation are discussed and sample heating caused by excessive laser power during Raman scattering measurements is emphasized. Besides, we show that anomalous Raman modes related to Se precipitates also occur in selenides, thus providing a general vision for better characterization of selenides and tellurides by means of Raman scattering measurements and for a better understanding of chalcogenides in general.

Introduction

Layered and bulk Se- and Te-based chalcogenides have been thoroughly studied for over a century. However, since the boom of graphene, the study of 2D materials has increased exponentially and strong interest has been aroused in Te-based chalcogenides for photonic and optoelectronic applications. Consequently, a number of studies have been carried out on tellurides with different structure-types and compositions with special interest in van der Waals compounds. Among the common experimental techniques used to characterize materials, Raman scattering plays an important role since it can efficiently detect subtle structural changes due to atomic rearrangements in a non-destructive way that allows *in situ* characterization of materials and devices. Therefore, any considerations regarding the performance and common trends found in the Raman spectra (RS) of bulk and layered materials are of fundamental importance for proper characterization of materials and devices.

Among the vast literature concerning Raman scattering studies on Te-based chalcogenides one can find RS that are very similar to many tellurides despite their different compositions and even crystalline structures.[1–35] Those RS show mainly two broad bands. The first and most intense band is observed between 119 and 130 cm^{-1}, while the second one is usually observed between 139 and 145 cm^{-1}. These Raman features found in different tellurides are hereafter named anomalous Raman modes (ARMs) and give rise to anomalous Raman spectra (ARS) that in some cases even prevent the observation of the normal or intrinsic Raman modes of the material.

In the light of the above considerations, several questions arise: What is the origin of the ARMs in tellurides? Can they be attributed to the same origin in all tellurides? How can they be formed? Why are ARMs so prominent in many RS so as to hide, in many cases, the normal or intrinsic Raman modes of the corresponding compounds?

In order to answer these questions and shed light on the origin of the ARMs in tellurides we have gone through the literature and found that there is an ongoing controversy

[a] Instituto de Diseño para la Fabricación y Producción Automatizada, MALTA Consolider Team, Universitat Politècnica de València, 46022 Valencia, Spain. E-mail: fjmanjon@fis.upv.es
[b] Departamento de Física, Instituto de Materiales y Nanotecnología, MALTA Consolider Team, Universidad de La Laguna, 38205 Tenerife, Spain
[c] Faculty of Chemical Technology, University of Pardubice, Pardubice 532 10 Czech Republic
[d] Departamento de Física Aplicada i Electromagnetismo, Universitat de València, 46100 Burjassot, Spain
[e] Institut für Mineralogie, Kristallographie und Materialwissenschaft, Universitat Leipzig, Germany

† Electronic supplementary information (ESI) available. See DOI: 10.1039/d1tc00980j

regarding the origin of the ARMs. In order to solve this controversy, we have performed a joint experimental and theoretical vibrational study on several tellurides. Raman-active mode frequencies obtained from Raman scattering measurements performed on several bulk tellurides have been compared to *ab initio* theoretical simulations. Our study concludes that the ARMs common to many Te-based chalcogenides come from Te clusters or precipitates in the form of layers or grains of nanometric or micrometric size that eventually could dominate the RS, especially in nanometric 2D tellurides. Moreover, our study also provides proof that ARMs coming from Se precipitates are observed in selenides too.

Experimental and theoretical details

Bulk single crystals and polycrystalline samples with thickness larger than 50 mm were used in this work. Monoclinic GaTe, orthorhombic Sb_2Se_3 and rhombohedral GaGeTe, Bi_2Se_3 and Bi_2Te_3 were grown by the Bridgman method,[36–38] $SnBi_2Te_4$ was prepared in a silica glass ampoule,[39] and monoclinic α-As_2Te_3[40] and trigonal Te samples were commercially acquired.

Raman scattering measurements on all samples were performed in backscattering geometry under ambient conditions in air using a 50× long-working distance objective (focus spot around 2 μm) coupled to a Horiba Jobin Yvon HR800 UV microspectrometer with a thermoelectrically cooled CCD camera. Raman signals were excited with a vertically-polarized HeNe laser (632.8 nm) of 20 mW power. Neutral density filters were used to excite samples at different laser powers from 20 mW down to 0.2 mW. Low powers below 1 mW were employed for most measurements to avoid damage to the samples while high powers were used to intentionally heat and cause damage to the samples. Ultra-low frequency measurements down to 10 cm^{-1} were carried out with a set of volume Bragg grating filters for the 632.8 nm line. Polarization in different configurations was achieved either by rotating the sample with respect to the incident polarized laser light or by placing horizontal and vertical polarizers (analyzer) prior to the entrance of the Raman signal into the spectrometer. Unpolarized Raman measurements indicate that no analyzer and no specific orientation of the sample were used. A 1200 lines per mm grating provided an experimental resolution of 1.6 cm^{-1}. Analysis of Raman spectra has been performed by taking the 520 cm^{-1} Raman line of Si as a reference, by substracting the corresponding background and by fitting Voigt profiles to the Raman peaks in which the Gaussian width is fixed to the experimental resolution.

Ab initio theoretical calculations were carried out within the framework of density functional theory (DFT)[41] with the Vienna *Ab initio* Simulation Package (VASP),[42] using the pseudopotential method and the projector augmented wave (PAW) scheme.[43,44] In this work, the generalized gradient approximation (GGA) with the Perdew–Burke–Ernzerhof (PBE) parametrization extended to the solid state (PBEsol) was used for the exchange and correlation energy.[45] Lattice-dynamical properties were obtained for the Γ-point using the direct-force constant approach.[46]

Results and discussion

In order to approach the problem, we show in Fig. 1 the RS of monoclinic GaTe and rhombohedral GaGeTe. Good agreement is found between the RS of Fig. 1a and e and those reported earlier in the literature.[36,37,47–49] Also good agreement is observed between the experimental and theoretical wavenumbers for the first-order Raman-active modes in both compounds (see the bottom tick marks in Fig. 1). These are called normal or intrinsic RS. Curiously, another kind of RS can be measured, typically at the edges of the same samples, that we call ARS (Fig. 1c and g). Moreover, even a mixture of the two different types of RS can be measured in rather uniform zones close to the edges of the same samples (Fig. 1b and f).

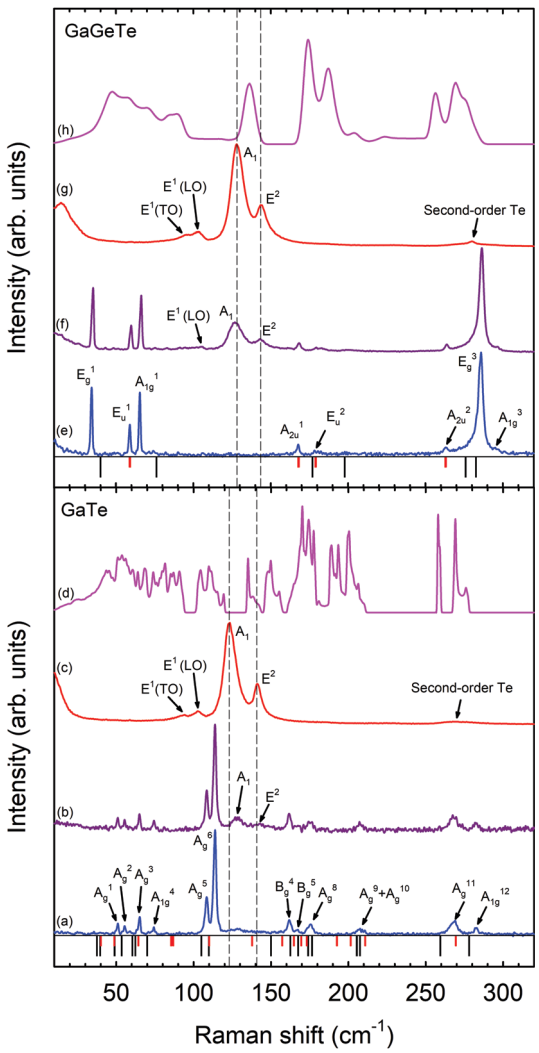

Fig. 1 Unpolarized RS of monoclinic GaTe and rhombohedral GaGeTe in different zones of the samples. (a) Normal RS of GaTe. (b) RS of GaTe with some ARMs. (c) ARS of GaTe. (d) Theoretical one-phonon density of states of GaTe. (e) Normal RS of GaGeTe. (f) RS of GaGeTe with some ARMs. (g) ARS of GaGeTe. (h) Theoretical one-phonon density of states of GaGeTe. The bottom black (red) tick marks show the calculated Raman-active (IR-active) TO modes of GaTe and GaGeTe. The dashed lines show the positions of the ARMs. The spectra have been normalized and vertically shifted for the sake of comparison and clarity.

It can be noticed that the normal RS of GaTe and GaGeTe have nothing in common; however, the ARS of the two samples look rather similar despite the different composition and crystalline structure of both compounds. The Raman bands shown in these RS are considered to be the ARMs common to all tellurides, so these RS are considered to be ARS from now on. As observed, the ARS of the two compounds show two intense and broad bands (one in the 122–128 cm^{-1} range and the other in the 141–144 cm^{-1} range). In fact, ARS measured on several regions of both samples evidence that these bands do not always have the same central wavenumbers (see Fig. 1b, c, f and g). In general, the first ARM in tellurides is usually located between 119 and 130 cm^{-1} and the second one is usually found between 139 and 145 cm^{-1}. In any case, the first band is always more intense and broader than the second one. In particular, the linewidth of those bands, defined by the full width at half maximum (FWHM), is found to be around 9.5 and 8 cm^{-1}, respectively, in Fig. 1c and g. A more detailed view of the ARS shows several weaker bands near 100 cm^{-1} and between 260 and 300 cm^{-1} that can also be considered as ARMs since they have been observed in other materials.[12,16,28]

The striking point is that most of the bands observed in the ARS of GaTe and GaGeTe, especially the two strongest ones, have been observed in a number of 2D and bulk Te-based chalcogenides with different laser wavelengths (typically from blue to red lasers), irrespective of their different compositions and crystalline structures. They have been observed in ZnTe,[1,2] CdTe,[3–8] GaTe,[9–16] As_2Te_3,[17] Sb_2Te_3,[18,19] Bi_2Te_3,[20,21] GeTe,[22,23] SnTe and PbTe,[24,25] $GeTe_2$,[26–29] $TiTe_2$,[30–33] GaGeTe,[49] $SnSb_2Te_4$,[34] and crystalline $Ge_2Sb_2Te_5$,[35] to name a few. Therefore, one wonders about the origin of the ARMs in tellurides.

To give answers to the questions already posed, we have gone through the literature and found that there is an ongoing controversy regarding the nature of the ARMs. Many authors generally attribute them to the intrinsic Raman modes of the sample or simply to oxidation. In the first explanation, they have been attributed either to Raman-active modes of the material or to IR-active modes of the material that are observed in Raman scattering measurements due to the breakdown of Raman selection rules. Unfortunately, this explanation cannot account for the ARMs either in GaTe or in GaGeTe (see the theoretically predicted Raman- and IR-active modes in both compounds as tick marks in Fig. 1). In monoclinic GaTe, IR-active modes are not observed in the RS and the calculated IR-active modes have wavenumbers that do not match with those of the two ARMs. Moreover, the theoretically calculated Raman-active modes for the other known polymorph of GaTe, hexagonal GaTe, either in monolayer or bulk form[50] do not match with the ARMs. On the contrary, many IR-active modes are observed in the RS of GaGeTe[49,51] and match with the theoretically calculated values. Therefore, we can conclude that this explanation for the origin of the ARMs is not consistent. In fact, similar Raman- or IR-active modes cannot be observed in all tellurides with such different compositions and crystalline structures. Consequently, a different origin must be invoked for the ARMs in all tellurides.

Surface oxidation has also been proposed in many papers to explain the origin of the ARMs in tellurides. In some studies, ARMs have been specifically attributed to the formation of TeO_2 layers. In this context, it is well known that the three known polymorphs of TeO_2 under ambient conditions show narrow and intense Raman bands in a wide wavenumber region, with several strong peaks below 250 cm^{-1}, near 400 cm^{-1} and above 600 cm^{-1}.[52–54] Consequently, the Raman modes of the TeO_2 polymorphs are not consistent with the observed and reported ARMs in tellurides,[24,25] as already noted in studies that confirmed the presence of TeO_2 surface layers by X-ray photoelectron spectroscopy.[24] In addition, it must be noted that the 62 cm^{-1} mode characteristic of paratellurite, the most stable phase of TeO_2, was observed in the RS of supposedly amorphous Te (later attributed to TeO_2) obtained from melting due to the use of a relatively high laser power (125 mW) during Raman scattering measurements of pure trigonal Te.[52,55] However, such a Raman mode has not been observed on a regular basis either in any of the ARS of tellurides already discussed or in our RS of GaTe and GaGeTe. Therefore, the formation of TeO_2 layers in tellurides cannot be the origin of the ARMs in tellurides.

More recently, molecular oxygen adsorbed in the sample surface or in the first atomic layers due to sample oxidation has also been proposed as the origin of the ARMs in GaTe films.[12] In particular, vibrational modes of GaTe-O_2 have been suggested as the cause of the two broad Raman bands. Once again, we must note that it is unlikely that the same oxygen molecules give rise to the same ARS in all tellurides with different compositions and, more importantly, crystalline structures. We must note that among tellurides there are many layered van der Waals-type compounds with Te-terminating layers, but also non-layered compounds. Moreover, one can find layered van der Waals-type compounds showing flat layers (GeTe, Sb_2Te_3, GaGeTe, $SnSb_2Te_4$, and $SnBi_2Te_4$), irregular layers (GaTe) and zigzag layers (α-As_2Te_3), as well as non-layered compounds with zinc blende-like structure (ZnTe, CdTe, and HgTe) and with rocksalt-type structure (SnTe and PbTe). Thus, it is unlikely that the modes of GaTe-O_2, with O_2 molecules between the layers or at the surface, can equally account for the ARMs in all layered and non-layered tellurides.

In some recent papers, the ARMs in tellurides have been attributed to other causes. In a study of GaTe films,[9] the two main ARMs have been attributed to second-order Raman scattering due to the existence of a double resonance in GaTe, like that of $MoTe_2$ and graphene.[56,57] The large linewidth and small polarization dependence of the two main ARMs in tellurides were claimed to give support to the hypothesis of the double resonance in GaTe.[9] To complement the measurements already performed on GaTe, we have performed polarized and unpolarized Raman scattering measurements on GaGeTe (Fig. S1 in the ESI†) that indeed evidence that the main ARMs show a similar dependence on polarization, as already reported in the literature for ARMs like those observed in GaTe.[9] In any case, it is unlikely that the same double resonance mechanism (likely valid for $MoTe_2$, which does not show the two main ARMs of tellurides in ref. 56) is also valid for ZnTe, CdTe, HgTe,

GeTe, SnTe, PbTe, GaTe, $GeTe_2$, GaGeTe, and so on, whose crystalline structures and electronic band structures are completely different among them. We want to stress that, while this hypothesis could account for some second-order Raman modes in tellurides, like $MoTe_2$ with a bandgap around 1.1 eV,[56] it is rather unlikely that it can show similar resonances for GaTe, a semiconductor with a bandgap around 1.65 eV,[12] and GaGeTe, a semimetal with very small direct and indirect bandgaps.[58] We refer the reader to the theoretically calculated electronic band structures of monoclinic GaTe and rhombohedral GaGeTe that are reported in the Materials Project Database.[59,60] It can be observed that they are of a completely different nature, which makes improbable the observation of a double resonance in both compounds with similar features to those shown in Fig. 1. Moreover, it is very unlikely that resonances could occur by excitation with different laser wavelengths in such different tellurides as those already discussed. Therefore, the double resonance mechanism cannot be the explanation for the ARMs in so many tellurides and another explanation is required.

A Raman-active mode originating from an *M*-point Brillouin-zone-edge mode folded into the Brillouin-zone center (Γ-point) has also been recently proposed as the origin of the ARMs in $TiTe_2$.[32] Again, it is very unlikely that this explanation could also be valid for such different compounds, with completely different compositions and crystalline structures, thus giving completely different vibrational branches along the whole Brillouin zone. Fig. S2 in the ESI† shows the phonon dispersion curves of GaTe and GaGeTe. It can be observed that they are completely different and cannot yield similar ARS even by folding different Brillouin-edge points into the Γ-point. Consequently, another explanation for the ARMs in tellurides is needed.

Defects or disorder have also been claimed as the origin of the ARMs in GaTe films.[10,11] It is well known that defects or disorder result in RS showing local vibrational modes in addition to the intrinsic Raman modes of the corresponding material or being dominated either by the one-phonon density of states or by the observation of silent modes.[61] Regarding disorder, it can be seen that the one-phonon density of states of monoclinic GaTe and rhombohedral GaGeTe (Fig. 1d and h) does not agree either with the normal Raman modes or with the ARMs observed in either compound. This result proves that our samples are of good quality and that the ARMs do not come from disorder. In addition, there are no silent modes in the vibrational spectrum of GaTe and GaGeTe, so ARMs cannot correspond to silent modes activated by disorder. On the other hand, regarding defects or impurities, they can give rise to local vibrational modes, which usually are relatively narrow bands, unlike the broad bands shown in the ARS. Consequently, the disorder or defect origin of the ARMs can be discarded. In any case, we want to note that this hypothesis could be a possible explanation for the ARMs in some compounds, but again it does not provide an explanation for the origin of the ARMs in other compounds since completely different local vibrational modes, silent modes, and one-phonon density of states will be obtained for different tellurides with different composition and crystalline structure.

Finally, there are some studies in which a much simpler explanation is given for the origin of the ARMs in tellurides. They have been tentatively attributed to the presence of defects in the form of Te precipitates, *i.e.* grains or layers of pure trigonal Te segregated from the original sample.[1–3,5,8,17,24,34] Unlike in previous studies in which this hypothesis has been suggested, in this work we provide a number of arguments in order to strengthen this hypothesis as the most probable one to explain the origin of the ARMs in tellurides. For that purpose, we have first compared the ARS of GaTe and GaGeTe in Fig. 1 with the unpolarized RS of pure trigonal Te (Fig. 2). Moreover, unpolarized and polarized RS of crystalline trigonal Te are reported in Fig. S3 in the ESI† for comparison.

As regards our unpolarized and polarized RS of crystalline Te (Fig. S3, ESI†), they are similar to those reported in the literature[3,55,62–64] and show three main bands around 91, 120 and 140 cm^{-1} corresponding to the three first-order Raman modes E^1(TO), A_1 and E^2(TO) of trigonal Te. In this context, we have denoted the two E modes of trigonal Te with superindexes

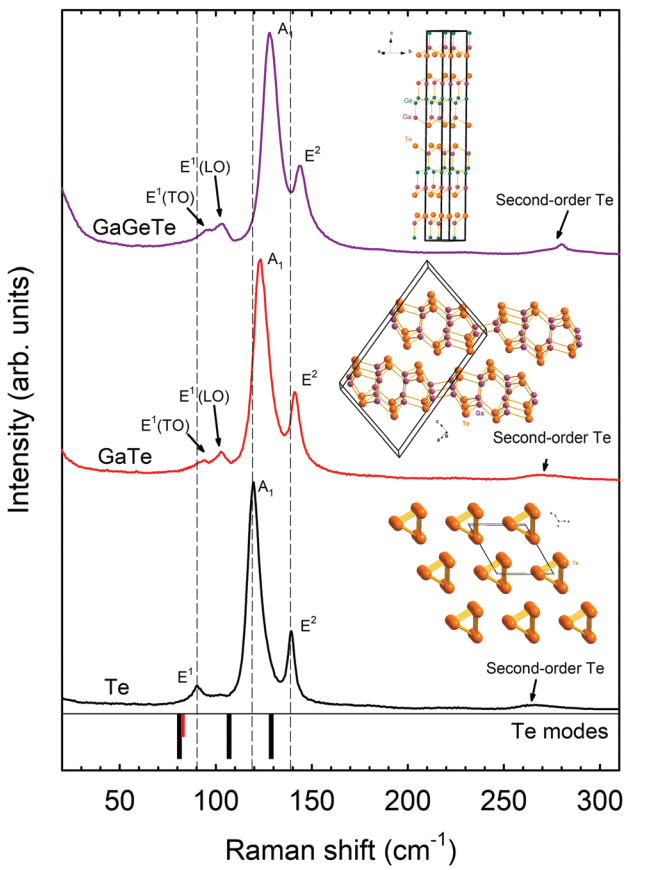

Fig. 2 Comparison of the unpolarized RS of Te and the unpolarized ARS of layered GaTe and GaGeTe. The bottom black tick marks show the calculated Raman-active TO modes of trigonal Te (E^1, A_1, and E^2). The bottom red tick marks show the calculated IR-active A_2(TO) mode of trigonal Te. Note that the E^1 and E^2 modes of Te are also IR-active, so the A_2, E^1 and E^2 modes can also show LO features. The spectra have been normalized and vertically shifted for the sake of comparison and clarity. The insets show the orientation of the layered samples during Raman measurements.

1 and 2 to distinguish the low and high-wavenumber E modes, respectively. Additionally, several weak bands attributed to the second-order modes of trigonal Te have been observed in good agreement with the literature, especially the broad band near 260 cm^{-1}.[55,65–67] The FWHM values of the E^1, A_1 and E^2 modes of trigonal Te are: 3.2(4), 4.8(2) and 2.8(3) cm^{-1}, respectively. It can be observed that the A_1 mode (the stronger mode) shows a larger linewidth than the two E modes. It can also be observed that the RS of trigonal Te are rather sensitive to the polarization when the laser polarization (E) is either parallel or perpendicular to the c axis; however, the Raman modes of Te show much smaller sensitivity to the polarization of the collected scattered light when the laser polarization is at 45° with respect to the c axis.

As regards Fig. 2, one can notice the strong similarity of the unpolarized RS for pure trigonal Te and the unpolarized ARS of GaTe and GaGeTe. All RS show two intense bands close to 120 and 140 cm^{-1}, weaker bands near 100 cm^{-1} and much weaker bands near 260 cm^{-1}. Therefore, all the ARMs in both tellurides could be attributed to the first-order modes (A_1, E^1(TO), E^1(LO), and E^2(TO)) and second-order modes of trigonal Te. A closer comparison between them shows that most ARMs in GaTe and GaGeTe, as well as in most tellurides,[1–35] are shifted to larger wavenumbers and are broader than those in pure trigonal Te. Additionally, the ARS of GaTe and GaGeTe exhibit one extra peak near 100 cm^{-1} and no sensitivity to polarization, as shown in Fig. S1 (ESI†). On top of that, the observation of the second-order Raman modes of Te above 260 cm^{-1}, as have been observed in the ARS of GaTe and GaGeTe, gives fundamental support to their assignment to Te precipitates. In fact, these modes have also been reported in some tellurides.[12,16,28] Noteworthy, a shift to larger wavelengths is observed for the second-order modes above 260 cm^{-1} in the ARS of tellurides compared to pure trigonal Te in good agreement with the shift of the first-order modes of Te. In summary, the ARMs in tellurides show strong similarities with those of pure trigonal Te, which suggests that they could come from Te precipitates, but they also show some differences that must be explained to further give support to this hypothesis.

The first difference to be explained is the blueshift of the wavenumbers of the Raman modes of Te in the ARS of tellurides. As we have already commented, the two main ARMs in Te-based chalcogenides occur at different wavenumbers around 119–130 cm^{-1} and 139–145 cm^{-1}.[1–35] In this respect, it has been shown that in general the Raman modes of trigonal Te shift to higher frequencies in 2D Te as the number of tellurene layers decreases.[68–72] In fact, values of the A_1 and E^2 modes as high as 136 and 149 cm^{-1}, respectively, have been measured in Te monolayers.[69] Only in one study were the Raman peaks found to shift first to larger wavenumbers and then to smaller wavenumbers in 2D Te as the number of layers decreases.[71] We can speculate that this strange Raman shift behavior is likely due the compressive stress on Te layers below a critical thickness. Consequently, we think that the larger wavelengths observed in the ARMs of tellurides with respect to bulk Te can be ascribed to the small layer thickness or grain size of polycrystalline Te precipitates (of the order of nm to μm) present in tellurides, as already observed in some earlier work on CdTe.[24] In fact, an estimation of the layer thickness or grain size of polycrystalline Te precipitates can be made on the basis of recent works.[68–72] According to these studies, flakes of pure Te between 10 and 30 nm showed the two bands around 124–125 and 143 cm^{-1}, respectively, while flakes with a thickness below 1 nm show bands at wavelengths above 129 and 147 cm^{-1}, respectively. Therefore, it can be concluded that ARMs in tellurides with similar or larger wavenumbers than those here mentioned can be considered to correspond to pure Te grains or layers of nanometric size.

In this context, it is interesting to note that, while the hardening of the E-type modes is expected in 2D materials in comparison to bulk materials, the large hardening of the A-type mode in 2D Te (contrary to that observed in other 2D materials) is still not fully understood in the context of the standard covalent and van der Waals forces of layered materials.[69]

The larger linewidth of the ARMs in tellurides than in pure trigonal Te can also likely be ascribed to the nanometric nature of the Te precipitates in tellurides. Note that Te nanoprecipitates, with grains of different sizes or layers of different thicknesses, will give rise, on one hand, to different wavenumbers for each Raman-active mode and, on the other hand, to broader linewidths due to the relaxation of Raman selection rules. Consequently, the RS of nanoprecipitates will result from the sum (convolution) of the Raman-active modes of Te precipitates with different grain sizes or layer thicknesses, thus resulting in much broader linewidths than in bulk trigonal Te. It must also be mentioned that the shift of the wavenumbers and broadening of ARMs in tellurides could also be partially attributed to strain in the segregated Te at the surface, as already suggested to occur in CdTe;[3] however, we think that this shift, which would depend on the lattice mismatch between pure Te and the corresponding telluride, will be a minor component in comparison to the shift caused by the nanometric nature of the precipitates.

Further support for the assignment of the ARMs in tellurides to Te precipitates is that both the E^1(TO) and E^1(LO) modes of Te are observed in the RS of both GaTe and GaGeTe. The E^1(LO) mode has a wavenumber around 104 cm^{-1} in good agreement with previous work on trigonal Te.[3,63,64] The observation of the E^1(LO) mode of Te has been made in 2D Te layers[69] and is likely due to the partial breakdown of the Raman selection rules in nanocrystalline-size Te precipitates. The lack of long range order in nanocrystalline-size grains allows the observation of IR-active modes in the RS.[73] In fact, the contribution of IR-active A_2 modes of trigonal Te to the broad band near 100 cm^{-1} in the ARS of GaTe and GaGeTe cannot be discarded.[63,64] It must also be noted that the observation of the LO modes of Te in the Raman spectra due to the breakdown of Raman selection rules in nanometric precipitates not only contributes to show the presence of the E^1(LO) mode but can also contribute to the broadening of the E^2 mode since both the E^2(TO) and E^2(LO) modes in trigonal Te show very similar wavelengths, unlike for the A_2 and E^1 modes.[55,63,64]

Another question to be answered is why the main ARMs in tellurides show such small polarization sensitivity unlike the

first-order modes of trigonal Te. The reason for the depolarized ARS in tellurides can also be ascribed to the formation of polycrystalline Te precipitates of very small and different grain sizes. All those small grains could be randomly oriented with respect to the polarized laser light so they give rise to completely depolarized RS. It is noteworthy that completely depolarized RS was assumed to be related to initially assumed amorphous Te obtained by laser melting and recrystallization of pure Te.[55] That RS was later attributed to paratellurite despite the fact that only one peak of paratellurite at 62 cm^{-1} was clearly found[52] in comparison with what was reported in the literature.[52–54] We think that laser melting of pure trigonal Te reported in ref. 55 resulted in Raman modes of 62, 120 and 146 cm^{-1} related to the formation of amorphous Te (Raman modes of 120 and 146 cm^{-1}) as well as of paratellurite (Raman mode of 62 cm^{-1} with some contribution to the 146 cm^{-1} mode) due to strong surface oxidation favoured by the high temperature reached upon excitation with 125 mW of laser power.

Several additional considerations support the assignment of the ARMs of tellurides to mainly nanocrystalline-size Te clusters or precipitates: (i) The two strongest modes of Te (A_1 and E^2) always appear as a pair in most ARS in tellurides. (ii) The intensity ratio of both ARMs is always similar to that found in trigonal Te. (iii) The FWHM of the first ARM is always larger than that of the second one as in trigonal Te and the FWHM of the two ARMs in Te precipitates is always larger than in pure Te as expected for layers of nanometric size. (iv) The two strongest ARMs measured in some tellurides, like ZnTe,[1] CdTe,[1] α-As_2Te_3,[17] and $SnSb_2Te_4$,[34] show negative pressure coefficients like those reported for bulk trigonal Te.[74–76] Moreover, the first ARM shows a larger negative pressure coefficient than the second one, as in trigonal Te.[1,17,34] In fact, the negative pressure coefficients shown by the ARMs are clear fingerprints of the Te nature of the ARMs in tellurides. Therefore, all the above mentioned features clearly indicate that the ARMs in tellurides are related to the formation of polycrystalline trigonal Te precipitates either in the form of nanocrystalline grains or layers. Since Te is common to all tellurides, Te segregation is a very reasonable hypothesis to explain the ARMs in such different tellurides as those discussed here. These segregates could be either in the interior of the material or at the surface of the samples.

Two questions still to be answered are why ARMs from trigonal Te clusters formed at the sample surface are so strong so as to hide the Raman signal of samples and how can they be observed even when TeO_2 films over Te layers have been found in several compounds. To answer these two questions we have to consider at least four factors: (i) TeO_2 polymorphs are insulating phases with large bandgaps (well above 2.5 eV),[77] so excitation of inner layers of Te below the TeO_2 layers is always possible because of the large penetration length of visible light in TeO_2. (ii) On the contrary, trigonal Te is a semimetal with a bulk bandgap around 0.33 eV and nanolayers have a much larger bandgap that can range from 0.65 to 1.17 eV.[78,79] With such small bandgaps for Te layers, excitation with visible light leads to a very small penetration depth as small as 500 Å (100 atomic layers).[80] Consequently, it is difficult to perform RS measurements of samples covered by a relatively thick Te layer, especially if the Raman signal of the sample is much smaller than that of trigonal Te. It is noteworthy that the formation of Te layers on top of or inside GaTe layers could explain not only the ARS but also the apparent decrease of the bandgap of GaTe (from 1.65 eV to 0.77 eV) when exposed to air.[12] (iii) It must be stressed that there is a strong resonance of the Raman modes of pure Te when excited with red and green laser lines that are usually employed for Raman scattering measurements in most laboratories.[63] Therefore, Te nanolayers have a fairly large Raman scattering cross section when excited with visible light that can avoid the observation of the Raman signal of samples below them. (iv) A much larger Raman scattering cross section was measured for the supposed amorphous Te than for bulk crystalline Te.[55] Therefore, the RS of Te thin films of nanometric size at the surface of samples show a strong signal that can even obscure the intrinsic Raman modes of the compound, as shown in the ARS of GaTe and GaGeTe in Fig. 1. In summary, all these factors can explain why ARMs are observed in many tellurides instead of the expected intrinsic Raman modes of the corresponding tellurides or in combination with them. Notable examples of Te modes obscuring the intrinsic Raman modes of certain compounds are recent RS measured in $TiTe_2$.[30–33] The recently reported RS of this compound are rather different to that previously reported[81] and surprisingly similar to those of trigonal Te, including the negative pressure coefficient of the two strongest Raman modes of Te.[32,33]

At this point, we must stress that our hypothesis of Te precipitates as the origin of the ARMs in Te-based chalcogenides is also valid for Se-based chalcogenides since ARMs due to Se segregation have also been observed in ZnSe,[1] CdSe,[8] $HgGa_2Se_4$,[82] $TiSe_2$,[83,84] $TaSe_2$[85] and In_2Se_3.[86] The ARMs in several of these selenides have been observed near 150 cm^{-1} (corresponding to the E^1 mode of trigonal Se) and/or near 235 cm^{-1} (the A_1 and E^2 modes of trigonal Se are sometimes overlapped near this wavenumber resulting in a strong Raman mode at room pressure). The mode near 235 cm^{-1} in trigonal Se is much stronger than that of 150 cm^{-1} and in many cases only the band near 235 cm^{-1} is observed in the ARS of selenides. Moreover, as in the case of tellurides, some ARMs due to Se nanoclusters have been found to shift with pressure with negative pressure coefficients[1,82,86] like those of bulk trigonal Se.[75,87,88] This feature is again a clear signature of Se-related modes. Therefore, our claim of trigonal Te precipitates being the cause of the ARMs in tellurides is also valid for selenides where Se precipitates have also been observed.

One additional question that must be clarified is how Se and Te precipitates can form in selenides and tellurides, respectively. In this context, we can comment on several factors for Se and Te segregation in chalcogenides. First of all, many selenides and tellurides are grown from the melt, where excess of Se and Te during crystal growth is usually present.[6] Therefore, Se and Te nanoclusters or few-layer films can occur during crystal growth,

especially near the sample edges, as proved in SnSe by positron annihilation spectroscopy.[89] It has also been proved that oxidation under ambient conditions seems to favour the presence of the ARMs.[12,15] On the other hand, it has also been shown that treatment with acid agents, like HCl, HF, and HNO_3, leads to formation of Te layers in CdTe, while dilution of bromine in methanol removes the Te layer.[3,5] High pressure has also been shown to favour sample decomposition and thus Se and Te segregation close to or after the occurrence of structural phase transitions.[1,34] Finally, the strong sensitivity of selenides and tellurides to light due to the large absorption coefficient of visible light in these compounds due to their small bandgaps is also well known. Therefore, excessive laser power during Raman scattering measurements can cause the decomposition of the samples and the segregation of Se and Te clusters or even the melting of the samples, as already reported with common lasers.[55]

In order to show the strong sensitivity of some tellurides to laser light during Raman scattering measurements and how ARMs in tellurides may occur upon excessive laser power irradiation, we have plotted in Fig. 3 the unpolarized RS of trigonal Te and other three tellurides (α-As_2Te_3, Bi_2Te_3 and $SnBi_2Te_4$) excited with different laser powers. It must be noted that excitation was performed with laser light (632.8 nm) having an energy of 1.98 eV, *i.e.* well above the bandgap of all these compounds, which are small-bandgap materials. As observed, the RS of trigonal Te (Fig. 3a) shows the main three Raman bands of Te at all laser powers. On the other hand, the RS of α-As_2Te_3 (Fig. 3b) and Bi_2Te_3 (Fig. 3c) excited with low power are similar to those already published[17,38,90] and the wavenumbers of the experimental modes match with those theoretically calculated (see the bottom marks in Fig. 3b and c). Finally, the RS of $SnBi_2Te_4$ is here reported for the first time to our knowledge and the Raman-active modes match those theoretically calculated (see the bottom marks in Fig. 3d). Note that the RS of $SnBi_2Te_4$ can be nicely compared to that recently published for isostructural $SnSb_2Te_4$.[34]

The Raman-active modes of Te redshift and broaden as the laser power is increased above 1 mW due to heating of the sample by excessive laser power during Raman scattering measurements (Fig. 3a). No signal of oxidation of the Te samples due to the formation of TeO_2 is observed with excitation power up to 20 mW. In fact, the RS excited with

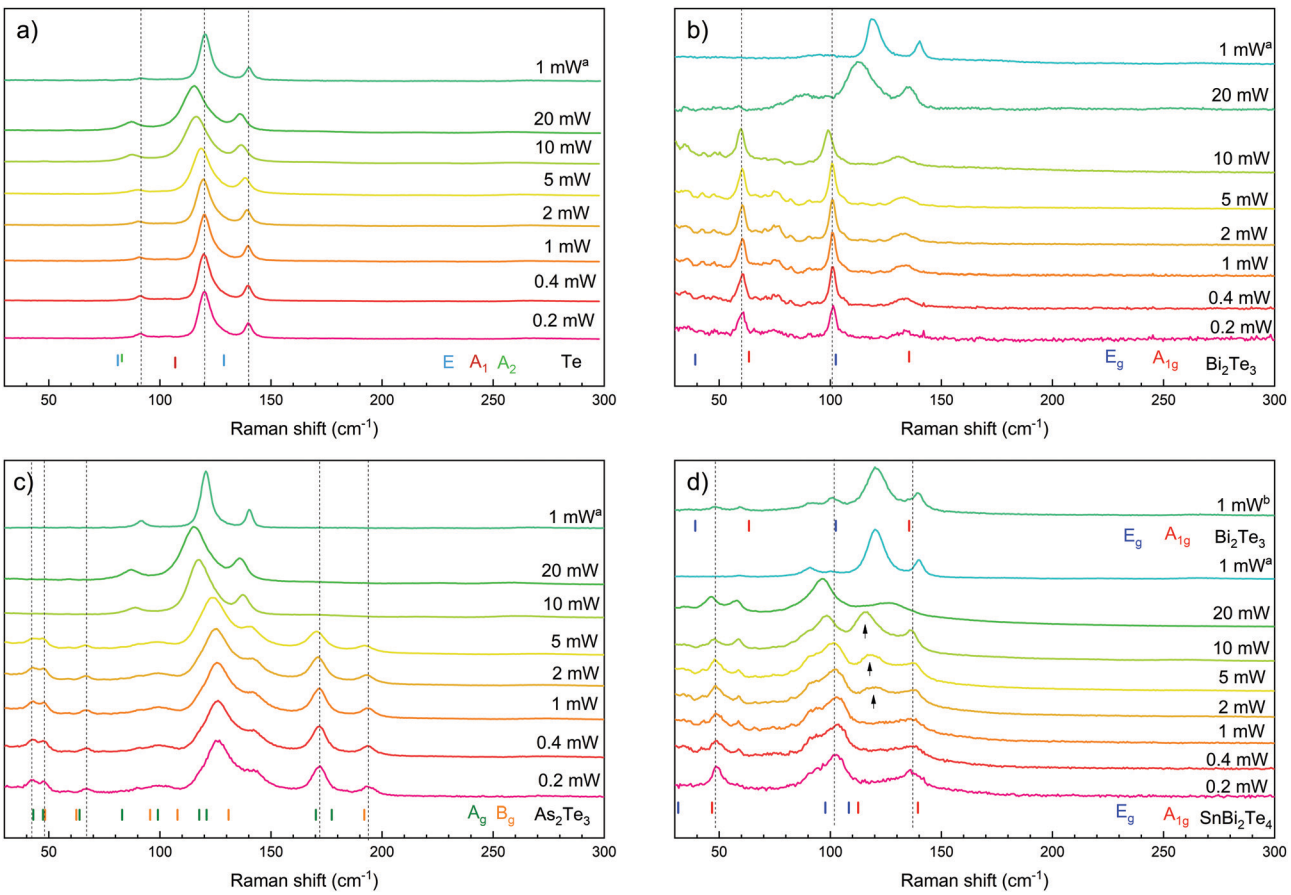

Fig. 3 Unpolarized RS of Te (a), Bi_2Te_3 (b), α-As_2Te_3 (c), and $SnBi_2Te_4$ (d) for different laser powers. The bottom black (red) tick marks show the calculated Raman-active (IR-active) TO modes of the different compounds. Some dashed lines, corresponding to the position of intrinsic Raman modes of the samples, have been added as guides to the eye. The spectra have been normalized and vertically shifted for the sake of comparison and clarity. The notation 1 mW^a and 1 mW^b indicates that those spectra have been excited with 1 mW power at the same spot previously excited with 20 mW once the sample has thermalized, but in different locations of the same sample.

1 mW laser power on the same spot of the sample previously heated once the sample is thermalized (see the top RS in Fig. 3a) shows again the same features observed in the RS obtained with low powers (see the bottom RS in Fig. 3a). A similar result is observed for GaGeTe heated by a laser (see the bottom and top of Fig. S4 in the SI). In this case, a redshift is observed for laser powers above 2 mW and no signals of Te or TeO_2 precipitates are observed even up to 20 mW, thus evidencing the high stability of the $R\bar{3}m$ phase of GaGeTe under laser irradiation. Therefore, it can be concluded that the ARMs of GaGeTe shown in Fig. 1 do not come from laser heating or from surface oxidation, but from surface or inner Te layers formed likely during bulk crystal growth.

A different scenario is found in α-As_2Te_3. Its RS shows, even at the smallest laser power, the two main ARMs around 126 and 142 cm^{-1}. They were previously reported and tentatively attributed to Te-related modes because of their negative pressure coefficients.[17] All the Raman bands of As_2Te_3 show a redshift on increasing the laser power above 1 mW due to sample heating by excessive laser power; however, a change in the RS can be observed for powers above 5 mW. Under these conditions, the Raman bands of As_2Te_3 disappear and only the ARS with the bands of trigonal Te are observed. Even the E^1(TO) mode close to 92 cm^{-1} and the second-order Raman mode of trigonal Te above 260 cm^{-1} are observed. In fact, the RS excited with 1 mW laser power on the damaged region due to excessive heating after proper thermalization shows the three first-order Raman peaks of trigonal Te located at 92, 121 and 140 cm^{-1}, *i.e.* at similar frequencies to those measured in pure bulk trigonal Te. Moreover, the FWHM values of the three peaks are 4.9, 5.2 and 3.1 cm^{-1}, respectively. These values of the wavenumbers and linewidths indicate that these ARMs in burned As_2Te_3 are closer to those of pure Te than to those observed in GaTe and GaGeTe in Fig. 1. Therefore, our results indicate that α-As_2Te_3 decomposes for powers above 5 mW and that excessive laser heating can lead to large Te clusters that can be considered almost bulk Te. Note that no signal of the E^1(LO) mode is observed in the RS of burned As_2Te_3, unlike in GaTe and GaGeTe. This is likely due to the validity of Raman selection rules in Te layers of rather large thickness or Te precipitates of rather large size formed at the surface of the burned sample.

In Bi_2Te_3, the Raman peaks redshift due to sample heating with increasing laser power above 5 mW and the shift of the Raman peaks occurs at a similar rate to that in GaGeTe, but at a much smaller rate than in As_2Te_3. The different redshift rates of Raman modes in these materials is likely due to the better thermal conductivity in Bi_2Te_3 and GaGeTe than in As_2Te_3 caused by the almost metallic nature (low bandgap) of the two former compounds. ARMs corresponding to trigonal Te were found only when excited with 20 mW laser power, thus evidencing the lower stability of the $R\bar{3}m$ phase of this compound under laser irradiation than in GaGeTe, but also its higher stability to laser irradiation than As_2Te_3. Again, the RS excited with 1 mW laser power over the damaged sample after proper thermalization (top RS in Fig. 3b) shows the two main Raman modes of pure trigonal Te located near 120 and 140 cm^{-1}, *i.e.* at similar wavenumbers to those measured in bulk Te. It must be noted that other rather stable tellurides seem to be Sb_2Te_3, $MoTe_2$ and WTe_2, in which trigonal Te modes have not been observed to our knowledge for any laser power irradiation or for different sample thicknesses in the literature. Once again it is shown that strong laser power can induce sample decomposition of Bi_2Te_3 and lead to big Te clusters.

As a final example of tellurides we show the RS of $SnBi_2Te_4$ (Fig. 3d), a compound that intrinsically shows cation disorder, as well as $SnSb_2Te_4$, even when synthesized by different routes.[91] All Raman bands redshift due to sample heating with increasing laser power above 1 mW. In fact, a change in the RS can be observed for laser powers above 2 mW, *i.e.* even at smaller powers than As_2Te_3. A broad Raman band close to 120 cm^{-1} appears that seems to correspond to trigonal Te; however, on further increasing the power we observed strong changes and the modes of Te are clearly shown at 20 mW plus some remnant low-frequency modes of the original sample. The RS excited with 1 mW on burned regions after proper thermalization but in two different sample locations show slightly different results. In some regions, the RS only shows the main bands of trigonal Te near 122 and 140 cm^{-1} (RS of 1 mW[a] in Fig. 3d), like in As_2Te_3 and Bi_2Te_3, while in other regions the Te modes are observed together with a band near 50 cm^{-1} that seems to correspond to original $SnBi_2Te_4$ and with two bands near 60 and 100 cm^{-1} that can be attributed to Bi_2Te_3 (RS of 1 mW[b] in Fig. 3d). In summary, our RS provide evidence of both Te segregation and decomposition of $SnBi_2Te_4$ into its parent compounds cubic SnTe and Bi_2Te_3 with increasing laser power. Since cubic SnTe does not show Raman modes, only those of Bi_2Te_3 are observed. This result agrees with the pressure-induced decomposition already observed in $SnSb_2Te_4$ upon compression.[34]

Finally, to further substantiate the idea that Se precipitates also occur in selenides, we have plotted in Fig. S5 (ESI†) the RS of two selenides (rhombohedral $R\bar{3}m$ Bi_2Se_3 and orthorhombic *Pnma* Sb_2Se_3) excited with different laser powers. Bi_2Se_3 shows a RS at low powers that is similar to that already reported[92] and is very stable to laser irradiation, like rhombohedral $R\bar{3}m$ Bi_2Te_3, with no signs of Se precipitates for any laser power, except in a region where a broad band near 250 cm^{-1} could be possibly attributed to Se when excited with a high power laser (RS of 1 mW[a] in Fig. S5a, ESI†). On the contrary, Sb_2Se_3 is rather sensitive to laser irradiation. At low power, the RS of the orthorhombic *Pnma* phase is observed in good agreement with the literature;[93–96] however, a completely different RS is observed above 5 mW together with some low-wavenumber peaks of the original *Pnma* phase of Sb_2Se_3. The RS excited with 1 mW laser power (RS of 1 mW[a] in Fig. S5b, ESI†) in the burned region after heat is dissipated shows that the new Raman peaks (see asterisk marks) correspond to the cubic phase of Sb_2O_3 (senarmontite).[95–97] This means that complete oxidation of the sample under air conditions is promoted by laser heating. Curiously, the RS obtained with 1 mW laser power close to the burned region (RS of 1 mW[b] in Fig. S5b, ESI†) show an

intense band above 230 cm^{-1}, that can be decomposed into two bands at 232 and 237 cm^{-1}, and a broad band between 430 and 500 cm^{-1}. Both the intense double mode and the broad band can be ascribed to the first-order Raman modes (A_1 and E^2) and to the second-order RS of trigonal Se, respectively.[66] Moreover, our results for Se segregation in Sb_2Se_3 and formation of cubic Sb_2O_3 at high laser powers are in agreement with recent works.[95,96] Therefore, our RS of Sb_2Se_3 clearly show that partial decomposition of the sample is observed and Se nanoclusters are segregated due to moderate laser heating.

As a final comment, we must note that ARMs in tellurides and selenides bear some differences. The main Raman band in Se nanoclusters of selenides is always located between 230 and 240 cm^{-1} and shows a very small Raman shift with respect to the bulk values. This is in clear contrast with the strong Raman shift of the A_1 mode in Te nanoclusters with respect to the bulk values. The small Raman shift in Se nanoclusters with respect to the bulk is in agreement with recently reported RS in few-layer Se sheets[98,99] and facilitates the identification of Se precipitates in selenides in comparison to Te precipitates in tellurides. In summary, our RS of selenides and tellurides with different excitation laser powers clearly show that care must be taken when exciting many of these compounds with laser powers higher than 1 mW. Laser powers below 1 mW must be used in order to avoid sample damage that can lead to partial or total decomposition of the chalcogenides and to segregation of Se and Te precipitates.

Conclusions

Anomalous Raman bands of rather high intensity and linewidth have been observed in Te-based binary and ternary chalcogenides, being the two strongest bands between 119 and 145 cm^{-1}. In the light of the results of Raman scattering measurements on telluride bulk materials and thin films, we have proposed a very reasonable explanation for the origin of the anomalous Raman modes in tellurides.

We consider that they come from the presence of polycrystalline Te clusters or precipitates either in the form of layers or grains (typically of nanometric size unless there is strong damage of the sample). They can be segregated at the first atomic layers of the sample surface but can also be formed inside the sample. Such segregation is usually found in as-grown bulk and 2D Te-based chalcogenides. Additional sources for the formation of pure Te precipitates can be oxidation, compression, and laser irradiation, *i.e.* processes that alter the delicate equilibrium of the stability of tellurides under ambient conditions.

We have also shown that a similar situation occurs for some Se-based chalcogenides where Se precipitates have been also found. Additionally, we have put special emphasis on the segregation of Se and Te precipitates due to the use of excessive laser power during Raman scattering measurements. Attention must be paid when performing Raman characterization of selenides and tellurides, especially for 2D materials and small samples with low thermal conductivity, where thermal radiation cannot be efficiently dissipated. In those cases, very low excitation powers below 1 mW (power density below 5 W/cm^2) are recommended for Raman scattering measurements to avoid sample heating and more notably Te and Se segregation.

We hope that the present work will help in interpreting the RS in selenides and tellurides in which the significance of the laser power must be taken into account for accurate and proper Raman characterization of these light-sensitive materials.

Author contributions

F. J. M. conceived the project, and planned and organized the experiments. S. G.-P. performed the measurements and analysed the data. P. R.-H. and A. M. performed the theoretical calculations. C. D., V. M.-S. and O. O. provided the studied samples. F. J. M. and S. G.-P. finalized the manuscript.

Conflicts of interest

There are no conflicts to declare.

Acknowledgements

This work has been performed under financial support from the Spanish Ministry of Science, Innovation and Universities, the Spanish Research Agency (AEI), and the European Fund for Regional Development (FEDER) under grants TEC2017-85912-C2-2, RED2018-102612-T (MALTA-CONSOLIDER TEAM network) and PID2019-106383 GB-C42/C43. We are also thankful for financial support from Generalitat Valenciana under grant PROMETEO/2018/123 (EFIMAT). The authors also acknowledge Dr Philipp Urban for performing the synthesis of $SnBi_2Te_4$.

References

1 G. Lindberg, R. Tallman, R. Lauck, M. Cardona, X. Liu, J. Furdyna and B. Weinstein, Effects of pressure on photo-induced formation of Se and Te clusters in II–VI compounds, *Phys. Stat. Sol. B*, 2013, **250**, 711–715, DOI: 10.1002/pssb.201200469.

2 L. N. Zhang, C. Liu, Q. M. Yang, L. J. Cui and Y. P. Zeng, Growth and characterization of highly nitrogen doped ZnTe films on GaAs(001) by molecular beam epitaxy, *Mater. Sci. Semicond. Process.*, 2015, **29**, 351–356, DOI: 10.1016/j.mssp.2014.06.045.

3 R. N. Zitter, Raman detection of tellurium layers on surfaces of CdTe, *Surf. Sci.*, 1971, **28**, 335–338.

4 S. H. Shin, J. Bajaj, L. A. Moudy and D. T. Cheung, Characterization of Te precipitates in CdTe crystals, *Appl. Phys. Lett.*, 1983, **43**, 68–70, DOI: 10.1063/1.94123.

5 P. M. Amirtharaj and F. H. Pollak, Raman scattering study of the properties and removal of excess Te on CdTe surfaces, *Appl. Phys. Lett.*, 1984, **45**, 789–791, DOI: 10.1063/1.95367.

6 N. Sochinskii, M. Serrano, E. Diéguez, F. Agulló-Rueda, U. Pal, J. Piqueras and P. Fernández, Effect of thermal annealing on Te precipitates in CdTe wafers studied by Raman scattering and cathodoluminescence, *J. Appl. Phys.*, 1995, **77**, 2806–2808, DOI: 10.1063/1.358687.

7 L.-j. Luan, W.-q. Jie, J.-j. Zhang and H.-c. Liu, Studies on Raman scattering and Te precipitates in cadmium manganese telluride, *J. Alloys Compd.*, 2009, **477**, 399–402, DOI: 10.1016/j.jallcom.2008.10.001.

8 Y. M. Azhniuk, V. V. Lopushansky, Y. I. Hutych, M. V. Prymak, A. V. Gomonnai and D. R. T. Zahn, Precipitates of selenium and tellurium in II–VI nanocrystal-doped glass probed by Raman scattering, *Phys. Stat. Sol. B*, 2011, **248**, 674–679, DOI: 10.1002/pssb.201046112.

9 S. Huang, Y. Tatsumi, X. Ling, H. H. Guo, Z. Q. Wang, G. Watson, A. A. Puretzky, D. B. Geohegan, J. Kong, J. Li, T. Yang, R. Saito and M. S. Dresselhaus, In-plane optical anisotropy of layered gallium telluride, *ACS Nano*, 2016, **10**, 8964–8972, DOI: 10.1021/acsnano.6b05002.

10 K. C. Mandal, T. Hayes, P. G. Muzykov, R. Krishna, S. Das, T. S. Sudarshan and S. Ma, Characterization of gallium telluride crystals grown from graphite crucible. Hard X-Ray, Gamma-Ray, and Neutron Detector Physics XII, *Proc. SPIE*, 2010, **7805**, 78050Q, DOI: 10.1117/12.863570.

11 K. C. Mandal, R. M. Krishna, T. C. Hayes, P. G. Muzykov, S. Das, T. S. Sudarshan and S. Ma, Layered GaTe crystals for radiation detectors, *IEEE Trans. Nucl. Sci.*, 2011, **58**, 1981–1986, DOI: 10.1109/TNS.2011.2140330.

12 J. J. Fonseca, S. Tongay, M. Topsakal, A. R. Chew, A. J. Lin, C. H. Ko, A. V. Luce, A. Salleo, J. Q. Wu and O. D. Dubon, Bandgap restructuring of the layered semiconductor gallium telluride in air, *Adv. Mater.*, 2016, **28**, 6465–6470, DOI: 10.1002/adma.201601151.

13 Q. Zhao, T. Wang, Y. Miao, F. Ma, Y. Xie, X. Ma, Y. Gu, J. Li, J. He, B. Chen, S. Xi, L. Xu, H. Zhen, Z. Yin, J. Li, J. Ren and W. Ji, Thickness-induced structural phase transformation of layered gallium telluride, *Phys. Chem. Chem. Phys.*, 2016, **18**, 18719–18726, DOI: 10.1039/C6CP01963C.

14 C. J. Bae, J. McMahon, H. Detz, G. Strasser, J. S. Park, E. Einarsson and D. B. Eason, Influence of thickness on crystallinity in wafer-scale GaTe nanolayers grown by molecular beam epitaxy, *AIP Adv.*, 2017, **7**, 035113, DOI: 10.1063/1.4978776.

15 J. Susoma, J. Lahtinen, M. Kim, J. Riikonen and H. Lipsanen, Crystal quality of two-dimensional gallium telluride and gallium selenide using Raman fingerprint, *AIP Adv.*, 2017, **7**, 015014, DOI: 10.1063/1.4973918.

16 Y. W. Yu, M. Ran, S. S. Zhou, R. Y. Wang, F. Y. Zhou, H. Q. Li, L. Gan, M. Q. Zhu and T. Y. Zhai, Phase-engineered synthesis of ultrathin hexagonal and monoclinic GaTe flakes and phase transition study, *Adv. Funct. Mater.*, 2019, **29**, 1901012, DOI: 10.1002/adfm.201901012.

17 V. P. Cuenca-Gotor, J. A. Sans, J. Ibáñez, C. Popescu, O. Gomis, R. Vilaplana, F. J. Manjón, A. Leonardo, E. Sagasta, A. Suárez-Alcubilla, I. G. Gurtubay, M. Mollar and A. Bergara, Structural, vibrational, and electronic study of α-As2Te3 under compression, *J. Phys. Chem. C*, 2016, **120**, 19340–19352, DOI: 10.1021/acs.jpcc.6b06049.

18 L. M. Goncalves, P. Alpuim, A. G. Rolo and J. H. Correia, Thermal co-evaporation of Sb2Te3 thin-films optimized for thermoelectric applications, *Thin Solid Films*, 2011, **519**, 4152–4157, DOI: 10.1016/j.tsf.2011.01.395.

19 D. T. Shi, R. P. Wang, G. X. Wang, C. Li, X. Shen and Q. H. Nie, Enhanced thermoelectric properties in Cu-doped Sb2Te3 films, *Vacuum*, 2017, **145**, 347–350, DOI: 10.1016/j.vacuum.2017.09.007.

20 V. Russo, A. Bailini, M. Zamboni, M. Passoni, C. Conti, C. S. Casari, A. Li Bassi and C. E. Bottani, Raman spectroscopy of Bi–Te thin films, *J. Raman Spectrosc.*, 2008, **39**, 205–210, DOI: 10.1002/jrs.1874.

21 C. Rodríguez-Fernández, C. V. Manzano, A. H. Romero, J. Martín, M. Martín-González, M. Morais de Lima Jr and A. Cantarero, The fingerprint of Te-rich and stoichiometric Bi2Te3 nanowires by Raman spectroscopy, *Nanotechnology*, 2016, **27**, 075706, DOI: 10.1088/0957-4484/27/7/075706.

22 C. Y. Khoo, H. Liu, W. A. Sasangka, R. I. Made, N. Tamura, M. Kunz, A. S. Budiman, C. L. Gan and C. V. Thompson, Impact of deposition conditions on the crystallization kinetics of amorphous GeTe films, *J. Mater. Sci.*, 2016, **51**, 1864–1872, DOI: 10.1007/s10853-015-9493-z.

23 R. Wang, W. Zhang, J. Momand, I. Ronneberger, J. E. Boschker, R. Mazzarello, B. J. Kooi, H. Riechert, M. Wuttig and R. Calarco, Formation of resonant bonding during growth of ultrathin GeTe films, *NPG Asia Mater.*, 2017, **9**, e396, DOI: 10.1038/am.2017.95.

24 J. A. Cape, L. G. Hale and W. E. Tennant, Raman scattering studies of monolayer-thickness oxide and tellurium films on PbSnTe, *Surf. Sci.*, 1977, **62**, 639–646, DOI: 10.1016/0039-6028(77)90106-6.

25 H. Z. Wu, C. F. Cao, J. X. Si, T. N. Xu, H. J. Zhang and H. F. Wu, Observation of phonon modes in epitaxial PbTe films grown by molecular beam epitaxy, *J. Appl. Phys.*, 2007, **101**, 103505, DOI: 10.1063/1.2714682.

26 H. Fukumoto, K. Tsunetomo, T. Imura and Y. Osaka, Structural changes of amorphous GeTe2 films by annealing (formation of metastable crystalline GeTe2 Films), *J. Phys. Soc. Jpn.*, 1987, **56**, 158–162, DOI: 10.1143/JPSJ.56.158.

27 K. Tsunetomo, T. Sugishima, T. Imura and Y. Osaka, Stability of metastable GeTe2 in thin films, *J. Non-Cryst. Solids*, 1987, **95**, 509–516, DOI: 10.1016/S0022-3093(87)80151-5.

28 B. Han, Y.-J. Kim, J.-M. Park, L. L. Yusup, J. Y. Shin and W.-J. Lee, Reaction mechanism for atomic layer deposition of germanium ditelluride thin films, *J. Nanosci. Nanotechnol.*, 2017, **17**, 3472–3476, DOI: 10.1166/jnn.2017.14044.

29 R. T. Ananth Kumar, H. A. Mousa, P. Chithra Lekha, S. T. Mahmoud and N. Qamhieh, Scrutiny of structural disorder using Raman spectra and Tauc parameter in GeTe2 thin films, *J. Phys.: Conf. Ser.*, 2017, **869**, 012018, DOI: 10.1088/1742-6596/869/1/012018.

30 J. M. Khan, C. M. Nolen, D. Teweldebrhan and A. A. Balandin, Properties of quasi-two-dimensional crystals of titanium ditelluride, *ECS Trans.*, 2010, **33**, 211–217, DOI: 10.1149/1.3485620.

31 K. Y. Ding, F. Rao, S. L. Lv, Y. Cheng, L. C. Wu and Z. T. Song, Low-energy amorphization of TiSb2Te5 phase change alloy induced by TiTe2 Nano-Lamellae, *Sci. Rep.*, 2016, **6**, 30645, DOI: 10.1038/srep30645.

32 V. Rajaji, U. Dutta, P. C. Sreeparvathy, S. Ch Sarma, Y. A. Sorb, B. Joseph, S. Sahoo, S. C. Peter, V. Kanchana and Ch Narayana, Structural, vibrational, and electrical properties of 1T−TiTe2 under hydrostatic pressure: Experiments and theory, *Phys. Rev. B*, 2018, **97**, 085107, DOI: 10.1103/PhysRevB.97.085107.

33 M. Zhang, X. Q. Wang, A. Rahman, Q. S. Zeng, D. Huang, R. C. Dai, Z. P. Wang and Z. M. Zhang, Pressure-induced topological phase transitions and structural transition in 1T-TiTe2 single crystal, *Appl. Phys. Lett.*, 2018, **112**, 041907, DOI: 10.1063/1.5012842.

34 J. Á. Sans, R. Vilaplana, E. Lora da Silva, C. Popescu, V. P. Cuenca-Gotor, A. Andrada-Chacón, J. Sánchez-Benitez, Ó. Gomis, A. L. J. Pereira, P. Rodríguez-Hernández, A. Muñoz, D. Daisenberger, B. García-Domene, A. Segura, D. Errandonea, R. S. Kumar, O. Oeckler, P. Urban, J. Contreras-García and F. J. Manjón, Characterization and decomposition of the natural van der Waals SnSb2Te4 under compression, *Inorg. Chem.*, 2020, **59**, 9900–9918, DOI: 10.1021/acs.inorgchem.0c01086.

35 K. S. Andrikopoulos, S. N. Yannopoulos, A. V. Kolobov, P. Fons and J. Tominaga, Raman scattering study of GeTe and Ge2Sb2Te5 phase-change materials, *J. Phys. Chem. Sol.*, 2007, **68**, 1074–1078, DOI: 10.1016/j.jpcs.2007.02.027.

36 J. Pellicer-Porres, F. J. Manjón, A. Segura, V. Muñoz, C. Power and J. Gonzalez, Optical absorption in GaTe under high pressure, *Phys. Rev. B*, 1999, **60**, 8871–8877, DOI: 10.1103/PhysRevB.60.8871.

37 C. Drasar, V. Kucek, L. Benes, P. Lostak and M. Vlcek, Thermoelectric properties and nonstoichiometry of GaGeTe, *J. Solid State Chem.*, 2012, **193**, 42–46, DOI: 10.1016/j.jssc.2012.03.030.

38 R. Vilaplana, O. Gomis, F. J. Manjón, A. Segura, E. Pérez-González, P. Rodríguez-Hernández, A. Muñoz, J. González, V. Marín-Borrás, V. Muñoz-Sanjosé, C. Drasar and V. Kucek, High-pressure vibrational and optical study of Bi2Te3, *Phys. Rev. B*, 2011, **84**, 104112, DOI: 10.1103/PhysRevB.84.104112.

39 R. Vilaplana, J. A. Sans, F. J. Manjón, A. Andrada-Chacón, J. Sánchez-Benítez, C. Popescu, O. Gomis, A. L. J. Pereira, B. García-Domene, P. Rodríguez-Hernández, A. Muñoz, D. Daisenberger and O. Oeckler, Structural and electrical study of the topological insulator SnBi2Te4 at high pressure, *J. Alloys Compd.*, 2016, **685**, 962–970, DOI: 10.1016/j.jallcom.2016.06.170.

40 V. P. Cuenca-Gotor, J. A. Sans, J. Ibáñez, C. Popescu, O. Gomis, R. Vilaplana, F. J. Manjón, A. Leonardo, E. Sagasta, A. Suárez-Alcubilla, I. G. Gurtubay, M. Mollar and A. Bergara, Structural, vibrational, and electronic study of α-As2Te3 under compression, *J. Phys. Chem. C*, 2016, **120**, 19340–19352, DOI: 10.1021/acs.jpcc.6b06049.

41 P. Hohenberg and W. Kohn, Inhomogeneous electron gas, *Phys. Rev.*, 1964, **136**, B864–B871, DOI: 10.1103/PhysRev.136.B864.

42 G. Kresse and J. Furthmüller, Efficiency of *ab initio* total energy calculations for metals and semiconductors using a plane-wave basis set, *Comput. Mater. Sci.*, 1996, **6**, 15–50, DOI: 10.1016/0927-0256(96)00008-0.

43 P. E. Blöchl, Projector augmented-wave method, *Phys. Rev. B*, 1994, **50**, 17953–17979, DOI: 10.1103/PhysRevB.50.17953.

44 G. Kresse and D. Joubert, From ultrasoft pseudopotentials to the projector augmented-wave method, *Phys. Rev. B*, 1999, **59**, 1758–1775, DOI: 10.1103/PhysRevB.59.1758.

45 J. P. Perdew, A. Ruzsinszky, G. I. Csonka, O. A. Vydrow, G. E. Scuseria, Z. Constantin, L. A. Zhou and K. Burke, Restoring the density-gradient expansion for exchange in solids and surfaces, *Phys. Rev. Lett.*, 2008, **100**, 136406, DOI: 10.1103/PhysRevLett.100.136406.

46 K. Parlinski, Computer Code Phonon. http://www.computingformaterials.com/index.html.

47 G. B. Abdullaev, L. K. Vodopyanov, K. R. Allakhverdiev, L. V. Golubev, S. S. Babaev and E. Y. Salaev, Raman spectra of α-GaTe single crystals, *Solid State Commun.*, 1979, **31**, 851–855, DOI: 10.1016/0038-1098(79)90402-2.

48 J. C. Irwin, B. P. Clayman and D. G. Mead, Long-wavelength phonons in GaTe, *Phys. Rev. B*, 1979, **19**, 2099–2105, DOI: 10.1103/PhysRevB.19.2099.

49 E. López-Cruz, M. Cardona and E. Martínez, Raman spectrum and lattice dynamics of GaGeTe, *Phys. Rev. B*, 1984, **29**, 5774–5777, DOI: 10.1103/PhysRevB.29.5774.

50 A. V. Bandura, A. V. Kovalenko, D. D. Kuruch and R. A. Evarestov, Lattice dynamics and thermodynamic properties of bulk phases and monolayers of GaTe and InTe: A comparison from first-principles calculations, *Eur. J. Inorg. Chem.*, 2021, 126–138, DOI: 10.1002/ejic.202000634.

51 The mechanism of the allowance of IR-active modes in the Raman spectrum of GaGeTe is out of the scope of the present work and will be treated in a forthcoming paper.

52 A. Pine and G. Dresselhaus, Raman scattering in paratellurite, TeO2, *Phys. Rev. B*, 1972, **5**, 4087–4093, DOI: 10.1103/PhysRevB.5.4087.

53 T. Sekiya, N. Mochida, A. Ohtsuka and M. Tonokawa, Normal vibrations of two polymorphic forms of TeO2 crystals and assignments of Raman peaks of pure TeO2 glass, *J. Ceram. Soc. Jpn.*, 1989, **97**, 1435–1440, DOI: 10.2109/jcersj.97.1435.

54 J. C. Champarnaud-Mesjard, S. Blanchandin, P. Thomas, A. Mirgorodsky, T. Merle-Méjean and B. Frit, Crystal structure, Raman spectrum and lattice dynamics of a new metastable form of tellurium dioxide: γ-TeO2, *J. Phys. Chem. Sol.*, 2000, **61**, 1499–1507, DOI: 10.1016/S0022-3697(00)00012-3.

55 A. Pine and G. Dresselhaus, Raman spectra and lattice dynamics of tellurium, *Phys. Rev. B*, 1971, **4**, 356–371, DOI: 10.1103/PhysRevB.4.356.

56 H. H. Guo, T. Yang, M. Yamamoto, L. Zhou, R. Ishikawa, K. Ueno, K. Tsukagoshi, Z. D. Zhang, M. S. Dresselhaus and R. Saito, Double resonance Raman modes in monolayer and few-layer MoTe2, *Phys. Rev. B*, 2015, **91**, 205415, DOI: 10.1103/PhysRevB.91.205415.

57 P. Venezuela, M. Lazzeri and F. Mauri, Theory of double-resonant Raman spectra in graphene: Intensity and line shape of defect-induced and two-phonon bands, *Phys. Rev. B*, 2011, **84**, 035433, DOI: 10.1103/PhysRevB.84.035433.

58 E. Haubold, A. Fedorov, F. Pielnhofer, I. P. Rusinov, T. V. Menshchikova, V. Duppel, D. Friedrich, R. Weihrich, A. Pfitzner, A. Zeugner, A. Isaeva, S. Thirupathaiah, Y. Kushnirenko, E. Rienks, T. Kim, E. V. Chulkov, B. Büchner and S. Borisenko, Possible experimental realization of a basic Z2 topological semimetal in GaGeTe, *APL Mater.*, 2019, **7**, 121106, DOI: 10.1063/1.5124563.

59 A. Jain, S. P. Ong, G. Hautier, W. Chen, W. D. Richards, S. Dacek, S. Cholia, D. Gunter, D. Skinner and G. Ceder, Commentary: The materials project: A materials genome approach to accelerating materials innovation, *APL Mater.*, 2013, **1**, 011002, DOI: 10.1063/1.4812323.

60 A. Jain, S. P. Ong, G. Hautier, W. Chen, W. D. Richards, S. Dacek, S. Cholia, D. Gunter, D. Skinner and G. Ceder, Commentary: The materials project: A materials genome approach to accelerating materials innovation, *APL Mater.*, 2013, **1**, 011002, DOI: 10.1063/1.4812323.

61 F. J. Manjón, B. Marí, J. Serrano and A. H. Romero, Silent Raman modes in zinc oxide and related nitrides, *J. Appl. Phys.*, 2005, **97**, 053516, DOI: 10.1063/1.1856222.

62 B. Torrie, Raman spectrum of tellurium, *Solid State Commun.*, 1970, **8**, 1899–1901, DOI: 10.1016/0038-1098(70)90343-1.

63 W. Richter, Extraordinary phonon Raman scattering and resonance enhancement in tellurium, *J. Phys. Chem. Sol.*, 1972, **33**, 2123–2128, DOI: 10.1016/S0022-3697(72)80242-7.

64 G. Lucovsky, A comparison of the long wave optical phonons in trigonal Se and trigonal Te, *Phys. Stat. Sol. B*, 1972, **49**, 633–641, DOI: 10.1002/pssb.2220490226.

65 Z. J. Xie, C. Y. Xing, W. C. Huang, T. J. Fan, Z. J. Li, J. L. Zhao, Y. J. Xiang, Z. N. Guo, J. Q. Li, Z. G. Yang, B. Q. Dong, J. L. Qu, D. Y. Fan and H. Zhang, Ultrathin 2D nonlayered tellurium nanosheets: facile liquid-phase exfoliation, characterization, and photoresponse with high performance and enhanced stability, *Adv. Funct. Mater.*, 2018, **28**, 1705833, DOI: 10.1002/adfm.201705833.

66 P. J. Carroll and J. S. Lannin, Second order Raman-scattering in crystalline sulfur, selenium and tellurium, *J. Phys., Colloq.*, 1981, **42**, 643–645, DOI: 10.1051/jphyscol:19816187.

67 P. J. Carroll and J. S. Lannin, Vibrational properties of crystalline group-VI solids: Te, Se, S, *Phys. Rev. B*, 1983, **27**, 1028–1036, DOI: 10.1103/PhysRevB.27.1028.

68 H. O. H. Churchill, G. J. Salamo, S.-Q. Yu, T. Hironaka, X. Hu, J. Stacy and I. Shih, Toward single atom chains with exfoliated tellurium, *Nanoscale Res. Lett.*, 2017, **12**, 488, DOI: 10.1186/s11671-017-2255-x.

69 Y. X. Wang, G. Qiu, R. X. Wang, S. Y. Huang, Q. X. Wang, Y. Y. Liu, Y. C. Du, W. A. Goddard III, M. J. Kim, X. F. Xu, P. D. Ye and W. Z. Wu, Field-effect transistors made from solution-grown two-dimensional tellurene, *Nat. Electron.*, 2018, **1**, 228–236, DOI: 10.1038/s41928-018-0058-4.

70 A. Apte, E. Bianco, A. Krishnamoorthy, S. Yazdi, R. Rao, N. Glavin, H. Kumazoe, V. Varshney, A. Roy, F. Shimojo, E. Ringe, R. K. Kalia, A. Nakano, C. S. Tiwary, P. Vashishta, V. Kochat and P. M. Ajayan, Polytypism in ultrathin tellurium, *2D Mater.*, 2018, **6**, 015013, DOI: 10.1088/2053-1583/aae7f6.

71 R. A. Yadav, N. Padma, S. Sen, K. R. S. Chandrakumar, H. Donthula and R. Rao, Anomalous vibrational behavior of two dimensional tellurium: Layer thickness and temperature dependent Raman spectroscopic study, *Appl. Surf. Sci.*, 2020, **531**, 147303, DOI: 10.1016/j.apsusc.2020.147303.

72 Q. S. Wang, M. Safdar, K. Xu, M. Mirza, Z. X. Wang and J. He, van der Waals epitaxy and photoresponse of hexagonal tellurium nanoplates on flexible mica sheets, *ACS Nano*, 2014, **8**, 7497–7505, DOI: 10.1021/nn5028104.

73 J. Zi, H. Büscher, C. Falter, W. Ludwig, K. M. Zhang and X. D. Xie, Raman shifts in Si nanocrystals, *Appl. Phys. Lett.*, 1996, **69**, 200–202, DOI: 10.1063/1.117371.

74 W. Richter, J. Renucci and M. Cardona, Hydrostatic pressure dependence of first-order Raman frequencies in Se and Te, *Phys. Stat. Sol. B*, 1973, **56**, 223–229, DOI: 10.1002/pssb.2220840226.

75 K. Aoki, O. Shimomura, S. Minomura, N. Koshizuka and T. Tsushima, Raman scattering of trigonal Se and Te at very high pressure, *J. Phys. Soc. Jpn.*, 1980, **48**, 906–911, DOI: 10.1143/JPSJ.48.906.

76 C. Marini, D. Chermisi, M. Lavagnini, D. Di Castro, C. Petrillo, L. Degiorgi, S. Scandolo and P. Postorino, High-pressure phases of crystalline tellurium: A combined Raman and ab initio study, *Phys. Rev. B*, 2012, **86**, 064103, DOI: 10.1103/PhysRevB.86.064103.

77 S. Y. Guo, Z. Zhu, X. M. Hu, W. H. Zhou, X. F. Song, S. L. Zhang, K. Zhang and H. B. Zeng, Ultrathin tellurium dioxide: Emerging direct bandgap semiconductor with high-mobility transport anisotropy, *Nanoscale*, 2018, **10**, 8397–8403, DOI: 10.1039/C8NR01028E.

78 J. L. Chen, Y. W. Dai, Y. Q. Ma, X. Q. Dai, W. K. Ho and M. H. Xie, Ultrathin β-tellurium layers grown on highly oriented pyrolytic graphite by molecular-beam epitaxy, *Nanoscale*, 2017, **9**, 15945–15948, DOI: 10.1039/C7NR04085G.

79 J. S. Qiao, Y. H. Pan, F. Yang, C. Wang, Y. Chai and W. Jia, Few-layer tellurium: One-dimensional-like layered elementary semiconductor with striking physical properties, *Sci. Bull.*, 2018, **63**, 159–168, DOI: 10.1016/j.scib.2018.01.010.

80 T. Moss, Optical properties of tellurium in the infra-red, *Proc. Phys. Soc., Sect. B*, 1952, **65**, 62–66, DOI: 10.1088/0370-1301/65/1/309.

81 M. Hangyo, S.-I. Nakashima and A. Mitsuishi, Raman spectroscopic studies of MX2-type layered compounds, *Ferroelectrics*, 1983, **52**, 151–159, DOI: 10.1080/00150198308208248.

82 R. Vilaplana, O. Gomis, E. Pérez-González, H. M. Ortiz, F. J. Manjón, P. Rodríguez-Hernández, A. Muñoz, P. Alonso-Gutiérrez, M. L. Sanjuán, V. V. Ursaki and I. M. Tiginyanu, Lattice dynamics study of HgGa2Se4 at

high pressures, *J. Phys. Chem. C*, 2013, **117**, 15773–15781, DOI: 10.1021/jp402493r.

83 P. Goli, J. Khan, D. Wickramaratne, R. K. Lake and A. A. Balandin, Charge density waves in exfoliated films of van der Waals materials: Evolution of Raman spectrum in TiSe2, *Nano Lett.*, 2012, **12**, 5941–5945, DOI: 10.1021/nl303365x.

84 D. B. Lioi, D. J. Gosztola, G. P. Wiederrecht and G. Karapetrov, Photon-induced selenium migration in TiSe2, *Appl. Phys. Lett.*, 2017, **110**, 081901, DOI: 10.1063/1.4976745.

85 R. Samnakay, D. Wickramaratne, T. R. Pope, R. K. Lake, T. T. Salguero and A. A. Balandin, Zone-folded phonons and the commensurate–incommensurate charge-density-wave transition in 1T-TaSe2 thin films, *Nano Lett.*, 2015, **15**, 2965–2973, DOI: 10.1021/nl504811s.

86 J. Zhao and L. Yang, Structure evolutions and metallic transitions in In2Se3 under high pressure, *J. Phys. Chem. C*, 2014, **118**, 5445–5452, DOI: 10.1021/jp4076383.

87 H. Z. Liu, C. Q. Jin and Y. H. Zhao, Pressure induced structural transitions in nanocrystalline grained selenium, *Phys. B*, 2002, **315**, 210–214, DOI: 10.1016/S0921-4526(01)01100-0.

88 O. Degtyareva, E. R. Hernández, J. Serrano, M. Somayazulu, H.-K. Mao, E. Gregorianz and R. J. Hemley, Vibrational dynamics and stability of the high-pressure chain and ring phases in S and Se, *J. Chem. Phys.*, 2007, **126**, 084503, DOI: 10.1063/1.2433944.

89 K. Sraitrova, J. Cizek, V. Holy, T. Plechacek, L. Benes, M. Jarosova, V. Kucek and C. Drasar, Vacancies in SnSe single crystals in a near-equilibrium state, *Phys. Rev. B*, 2019, **99**, 035306, DOI: 10.1103/PhysRevB.99.035306.

90 W. Richter, H. Kohler and C. R. Becker, A Raman and far-infrared investigation of phonons in the rhombohedral V2–VI3 compounds Bi2Te3, Bi2Se3, Sb2Te3 and Bi2(Te1−xSex)3 ($0 < x < 1$), (Bi1−ySby)2Te3 ($0 < y < 1$), *Phys. Status Solidi B*, 1977, **84**, 619–628, DOI: 10.1002/pssb.2220840226.

91 R. Vilaplana, J. A. Sans, F. J. Manjón, A. Andrada-Chacón, J. Sánchez-Benítez, C. Popescu, O. Gomis, A. L. J. Pereira, B. García-Domene, P. Rodríguez-Hernández, A. Muñoz, D. Daisenberger and O. Oeckler, Structural and electrical study of the topological insulator SnBi2Te4 at high pressure, *J. Alloys Compd.*, 2016, **685**, 962–970, DOI: 10.1016/j.jallcom.2016.06.170.

92 R. Vilaplana, D. Santamaría-Pérez, O. Gomis, F. J. Manjón, J. González, A. Segura, A. Muñoz, P. Rodríguez-Hernández, E. Pérez-González, V. Marín-Borrás, V. Muñoz-Sanjosé, C. Drasar and V. Kucek, Structural and vibrational study of Bi2Se3 under high pressure, *Phys. Rev. B*, 2011, **84**, 184110, DOI: 10.1103/PhysRevB.84.184110.

93 Z. G. Ivanova, E. Cernoskova, V. S. Vassilev and S. V. Boycheva, Thermomechanical and structural characterization of GeSe2–Sb2Se3–ZnSe glasses, *Mater. Lett.*, 2003, **57**, 1025–1028, DOI: 10.1016/S0167-577X(02)00710-3.

94 I. Efthimiopoulos, J. Zhang, M. Kucway, C. Park, R. C. Ewing and Y. Wang, Sb2Se3 under pressure, *Sci. Rep.*, 2013, **3**, 2665, DOI: 10.1038/srep02665.

95 A. Shongalova, M. R. Correia, B. Vermang, J. M. V. Cunha, P. M. P. Salomé and P. A. Fernandes, On the identification of Sb2Se3 using Raman scattering, *MRS Commun.*, 2018, **8**, 865–870, DOI: 10.1063/1.4976745.

96 P. Vidal-Fuentes, M. Guc, X. Alcobe, T. Jawhari, M. Placidi, A. Pérez-Rodríguez and E. Saucedo, V. Izquierdo Roca, Multiwavelength excitation Raman scattering study of Sb2Se3 compound: Fundamental vibrational properties and secondary phases detection, *2D Mater.*, 2019, **6**, 045054, DOI: 10.1088/2053-1583/ab4029.

97 A. L. J. Pereira, L. Gracia, D. Santamaría-Pérez, R. Vilaplana, F. J. Manjón, D. Errandonea, M. Nalin and A. Beltrán, Structural and vibrational study of cubic Sb2O3 under high pressure, *Phys. Rev. B: Condens. Matter Mater. Phys.*, 2012, **85**, 174108, DOI: 10.1103/PhysRevB.85.174108.

98 J. K. Qin, G. Qiu, J. Jian, H. Zhou, L. M. Yang, A. Charnas, D. Y. Zemlyanov, C.-Y. Xu, X. F. Xu, W. Z. Wu, H. Y. Wang and P. D. Ye, Controlled growth of a large-size 2D selenium nanosheet and its electronic and optoelectronic applications, *ACS Nano*, 2017, **11**, 10222–10229, DOI: 10.1021/acsnano.7b04786.

99 T. J. Fan, Z. J. Xie, W. C. Huang, Z. J. Li and H. Zhang, Two-dimensional non-layered selenium nanoflakes: Facile fabrications and applications for self-powered photo-detector, *Nanotechnology*, 2019, **30**, 114002, DOI: 10.1088/1361-6528/aafc0f.